Primary energy spectrum as reconstructed from S(500) measurements by KASCADE-grande

(Article begins on next page)

25 August 2024

Primary Energy Spectrum as Reconstructed by KASCADE-Grande from *S*(500) Measurements

G. Toma[d], W.D. Apel[a], J.C. Arteaga[b,j], F. Badea[a], K. Bekk[a], M. Bertaina[c],
J. Blümer[a,b], H. Bozdog[a], I.M. Brancus[d], M. Brüggemann[e], P. Buchholz[e],
E. Cantoni[c,f], A. Chiavassa[c], F. Cossavella[b], K. Daumiller[a], V. de Souza[b,k],
F. Di Pierro[c], P. Doll[a], R. Engel[a], J. Engler[a], M. Finger[a], D. Fuhrmann[g], P.L. Ghia[f],
H.J. Gils[a], R. Glasstetter[g], C. Grupen[e], A. Haungs[a], D. Heck[a], J.R. Hörandel[b,l],
T. Huege[a], P.G. Isar[a], K.-H. Kampert[g], D. Kang[b], D. Kickelbick[e], H.O. Klages[a],
P. Łuczak[h], H.J. Mathes[a], H.J. Mayer[a], J. Milke[a], B. Mitrica[d], C. Morello[f],
G. Navarra[c], S. Nehls[a], J. Oehlschläger[a], S. Ostapchenko[a,m], S. Over[e], M. Petcu[d],
T. Pierog[a], H. Rebel[a], M. Roth[a], H. Schieler[a], F. Schröder[a], O. Sima[i],
M. Stümpert[b], G.C. Trinchero[f], H. Ulrich[a], A. Weindl[a],
J. Wochele[a], M. Wommer[a], J. Zabierowski[h]

[a] *Institut für Kernphysik, Forschungszentrum Karlsruhe, 76021 Karlsruhe, Germany*
[b] *Institut für Experimentelle Kernphysik, Universität Karlsruhe, 76021 Karlsruhe, Germany*
[c] *Dipartimento di Fisica Generale dell'Università, 10125 Torino, Italy*
[d] *National Institute of Physics and Nuclear Engineering, 7690 Bucharest, Romania*
[e] *Fachbereich Physik, Universität Siegen, 57068 Siegen, Germany*
[f] *Istituto di Fisica dello Spazio Interplanetario, INAF, 10133 Torino, Italy*
[g] *Fachbereich Physik, Universität Wuppertal, 42097 Wuppertal, Germany*
[h] *Soltan Institute for Nuclear Studies, 90950 Lodz, Poland*
[i] *Department of Physics, University of Bucharest, 76900 Bucharest, Romania*
[j] *now at: Universidad Michoacana, Morelia, Mexico*
[k] *now at: Universidade de São Paulo, Instituto de Fîsica de São Carlos, Brasil*
[l] *now at: Dept. of Astrophysics, Radboud University Nijmegen, The Netherlands*
[m] *now at: University of Trondheim, Norway*

Abstract. In cosmic ray investigations by observations of extensive air showers (EAS) the general question arises how to relate the EAS observables registered on ground to the energy of the primary particle from the cosmos entering into the atmosphere. We present results on the reconstruction of the primary energy spectrum of cosmic rays from the experimentally recorded *S*(500) observable using the KASCADE-Grande detector array The KASCADE-Grande experiment is installed in Forschungszentrum Karlsruhe, Germany, and driven by an international collaboration. Previous EAS investigations have shown that the charged particle density becomes independent of the primary mass at certain fixed distances from the shower core. This feature can be used as an estimator for the primary energy. The particular radial distance from the shower core where this effect takes place is a characteristic of the detector. For the KASCADE-Grande experiment it was shown to be around 500 m, hence a notation *S*(500) is used for the charged particle density at this specific distance. Extensive simulation studies have shown that *S*(500) is mapping the primary energy. The constant intensity cut (CIC) method is applied to evaluate the attenuation of the *S*(500) observable with the zenith angle. A correction is subsequently applied and all recorded *S*(500) values are corrected for attenuation, leading to the all event *S*(500) spectrum. A calibration of *S*(500) values with the primary energy has been worked out by simulations and has been used for conversion providing the possibility to obtain the primary energy spectrum (in the energy range accessible to the KASCADE-Grande array, 10^{16}-10^{18} eV). The systematic uncertainties induced by different factors are considered.

INTRODUCTION

Historically, the KASCADE-Grande detector array (at Forschungszentrum Karlsruhe, Germany, 110 m a.s.l.) [3] is an extension of a smaller array, the KASCADE array, operated since 1996. KASCADE was designed to record air showers initiated by primaries with energies in the 10^{14}-10^{16} eV range (including the knee range whose origin to clarify was one of the goals). The KASCADE detector is a complex detector array providing information on a considerable number of observables associated with the electromagnetic, muonic and hadronic component. The extension of the original smaller but rather detailed KASCADE array was guided by the intention to extend the energy range for efficient EAS detection to the energy range of 10^{16}-10^{18} eV. This energy range provides various interesting aspects: the expected transition from galactic to extragalactic cosmic rays and, in particular the question whether there exists a further "knee" in the energy spectrum (induced by the iron component when escaping from our Galaxy).

Hillas has shown that the EAS particle density distributions at a certain distance from the shower core (dependent on the EAS detection array) becomes independent of the primary mass and can be used as a primary energy estimator [1]. A method was derived to reconstruct the primary energy spectrum from the particular value of the charged particle density, observed at such specific radial ranges. The technique has been used by different detector arrays in order to reconstruct the primary energy spectrum of the cosmic radiation [2]. In the case of the KASCADE-Grande array, detailed simulations [4] have shown that the particular distance for which this effect takes place is about 500 m (see fig. 1). Therefore an observable of interest in the case of KASCADE-Grande is the charged particle density at 500 m distance from the shower core, noted as $S(500)$ in the following.

The reconstruction procedure uses the energy deposits of particles in the KASCADE-Grande detector stations and the associated temporal information (arrival times of particles). Using appropriate (angle-dependant [6]) **L**ateral **E**nergy **C**orrection **F**unctions (**LECF**), the energy deposits are converted into particle densities. A Linsley [7] **L**ateral **D**ensity **F**unction (**LDF**) is employed in order to evaluate the particle density at the radial range of interest, 500 m. The study has been performed for both simulated (fig. 1) and experimental (fig. 2) events, using identical reconstruction procedures [5]. The Monte-Carlo CORSIKA EAS simulation tool was used to simulate air showers (with QGSJET II model embedded for high energy interactions).
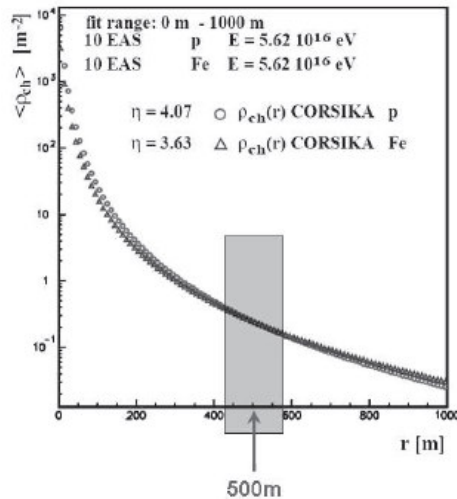

FIGURE 1. Simulations show that, for the case of the KASCADE-Grande experimental layout, the particle density becomes independent of the primary mass around 500 m distance from shower core; this plot shows averaged simulated lateral distributions for different primary types with equal energy.

EFFICIENCY AND QUALITY CUTS

Showers were detected on a 500 x 600 m^2 area up to 30° zenith angle during ~902 days of continuous acquisition. Analysis was performed up to 30° zenith angle in order to limit certain systematic effects affecting the reconstruction of small showers above this threshold. In order to ensure good reconstruction quality, several (same) quality cuts were imposed on both the experimental and simulated data. Only those events are accepted for which the reconstructed shower core is positioned inside the detector array and not too close to the border. A good quality of the fit to the Linsley distribution is a further important criterion. Fig. 3 shows the total reconstruction efficiency for different zenith angle intervals (the full efficiency is reached at around $\log_{10}(E_0/\mathrm{GeV})=7.5$).
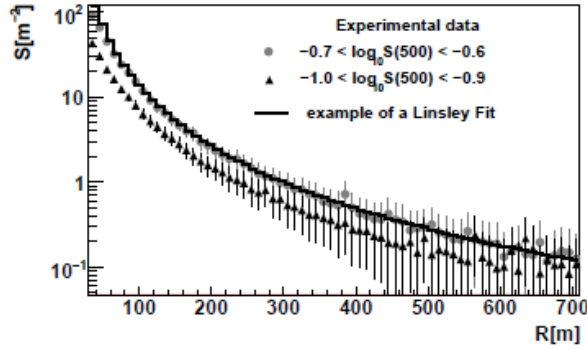
FIGURE 2. Averaged lateral density distributions of experimentally recorded EAS samples for two $S(500)$ ranges.
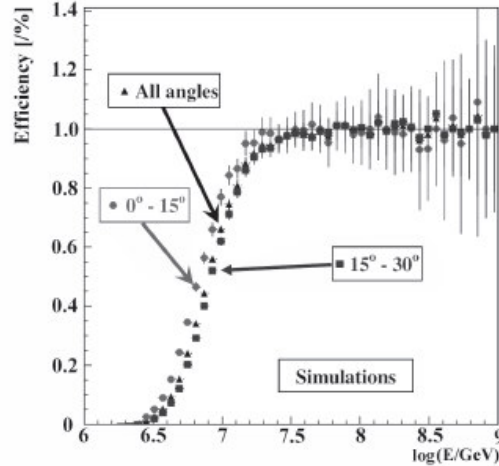
FIGURE 3. Simulations: reconstruction efficiency for different zenith angle ranges and for the entire shower sample (events triggering more than 24 stations).

THE CONSTANT INTENSITY CUT METHOD

For more inclined showers, the EAS particles have to cross a longer path through the atmosphere before reaching the detector level. In such a case, events generated by identical primaries reach the detector level at different stages of EAS development, dependent on their angles of incidence. As a consequence, for a given event sample, an EAS observable could have different values for events induced by identical primaries but arriving from different zenith angles. It is also the case of the S(500). One has to correct this effect before performing an analysis simultaneously on all EAS events. This is achieved by applying the **C**onstant **I**ntensity **C**ut (**CIC**) method. The attenuation of $S(500)$ is visible in fig. 4 where $S(500)$ spectra are plotted for different EAS incident angles. The angular intervals are

chosen in a way that they open equal solid angles: $0°-13.2°$, $13.2°-18.8°$, $18.8°-23.1°$, $23.1°-26.7°$ and $26.7°-30.0°$. $S(500)$ spectra are shifting towards lower values (attenuated) for increasing zenith angles. The CIC method assumes that a given intensity value in the energy spectrum corresponds to a given primary energy of particles and, since the $S(500)$ is mapping the primary energy spectrum, it is expected that this property of the intensity is true also in the case of $S(500)$ spectra. Therefore a constant intensity cut on integral $S(500)$ spectra is performed, effectively cutting them at a given primary energy. It is thus easy to establish a correspondence (in the form of an attenuation curve) between the attenuated $S(500)$ value and the angle of incidence for a given spectral intensity. The attenuation curve is parameterized and all reconstructed $S(500)$ values are corrected for attenuation by bringing them to the value they would have at a chosen reference angle (see fig. 5). Since $S(500)$ spectra are parallel for different zenith angles, various constant intensity cuts performed at different intensities will give parallel attenuation curves any of which could be used for constructing an attenuation correction (the parameterization with the lowest chi^2 was chosen, namely the one corresponding to intensity 3000). For the present study the reference angle is considered to be $21°$, since the zenith angular distribution for the recorded EAS sample peaks at this value.

The various mathematical transformations of the data implied by the CIC method introduce some systematic uncertainties on the final result of the CIC method. The CIC-induced systematic uncertainty of the corrected $S(500)$ value is evaluated by propagating the errors of fit parameters. The resulting CIC-induced error of the $S(500)$ observable will be taken into account later when evaluating the total systematic uncertainty of the reconstructed primary energy.
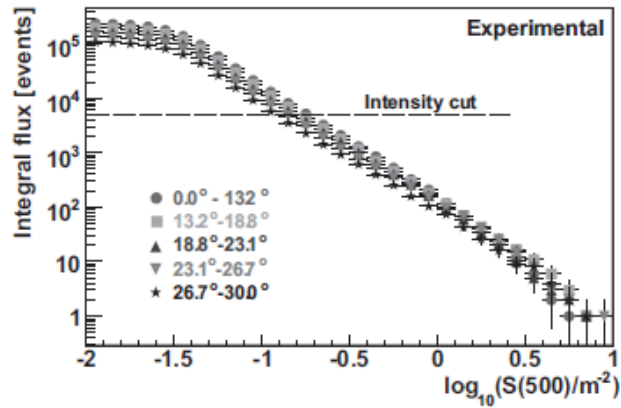

FIGURE 4. Integral $S(500)$ spectra; the horizontal line is a constant intensity cut at an arbitrarily chosen intensity; attenuation length of $S(500)$ was evaluated at 347.38 ± 21.65 g·cm^{-2}
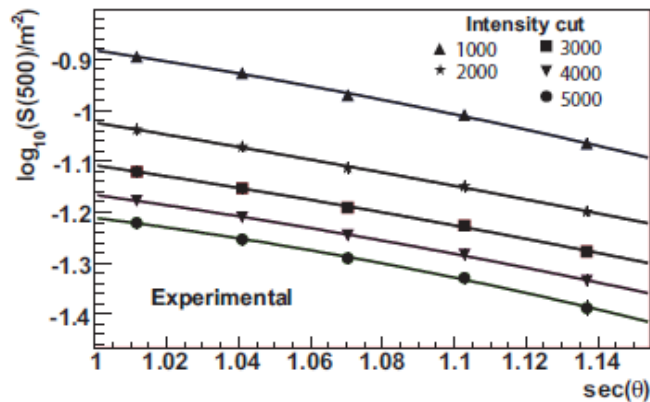

FIGURE 5. Attenuation of the $S(500)$ observable with the angle of incidence; the different curves show different arbitrarily chosen intensity cuts.
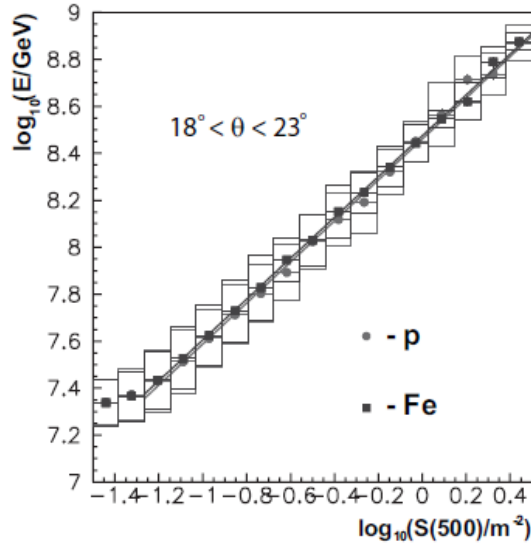
FIGURE 6. E_0 - $S(500)$ calibration curve for two different primaries; the box-errors are the errors on the spread; the errors on the mean are represented with bars.

CONVERSION TO ENERGY

A simulation-derived calibration of the primary energy E_0 with $S(500)$ was employed in order to convert the recorded $S(500)$ values into corresponding energy values (see fig. 6). The two slightly different dependencies in fig. 6 are representative for a light primary (proton) and a heavy primary (Fe). The two dependencies are nearly mass insensitive, a feature that derives from the properties of the $S(500)$ observable which is also supposed to be mass insensitive. Such a calibration is used to convert all $S(500)$ values into the corresponding primary energies leading to the reconstructed primary energy spectrum. Fig. 7 shows the reconstructed energy spectrum compared with spectra reconstructed by other experiments. For the systematic contribution to the total error, several sources of systematic uncertainties have been identified and their contributions were evaluated. Thus, the spectral index of the simulated shower sample (equal to -2) was acting as a source of systematic uncertainty. In a similar fashion, the $S(500)$-E_0 calibration and the CIC method itself were also introducing systematic uncertainties. In all, these three sources were contributing with an uncertainty of ~1% from the total flux value. Other sources that were considered were the Monte-Carlo statistical uncertainty of the simulated shower sample and the choosing of a certain reference angle at which to perform the $S(500)$ attenuation correction (contributing with ~7% and ~30% relative uncertainty). The relative contribution of all identified sources over the full efficiency range was fairly constant for any given source and in total amounts for about 37% of the recorded flux value. The energy resolution has been evaluated from simulations by calculating the difference between the true and the reconstructed primary energy and was found to be 22% for $E_0 = 10^{17}$ eV (for all primaries) (a value which is fairly constant over the entire full efficiency range).

CONCLUSIONS

With the phenomenon of Extensive Air Showers we have the opportunity to indirectly investigate the properties of the primary cosmic radiation for energies above the 10^{14} eV threshold where the primary flux becomes so low that direct observation is no longer practical. Thus, by recording measurable properties of EAS events (commonly called observables) we usually try to infer information on two main features of the primary radiation: its mass composition and energy. The work presented in this paper was directed at reconstructing the primary energy spectrum of cosmic rays. The charged particle density at 500 m distance from shower core was found to be a good energy estimator for the case of the KASCADE-Grande detector array. The S(500) has been recorded experimentally for a set of EAS events and, with the aid of simulations, it has been converted into primary energy. Attenuation effects were corrected by the use of the constant intensity cut method and several sources of systematic uncertainties have been

identified and their contribution to the overall uncertainty was evaluated. The same study was performed also on simulated events and thus an evaluation of energy resolution for the applied method was possible.
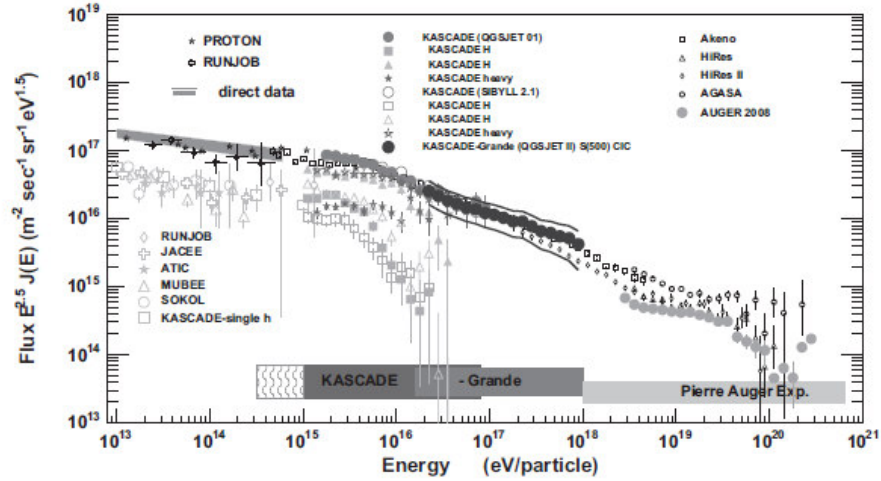

FIGURE 7. Reconstructed experimental energy spectrum by KASCADE-Grande from $S(500)$/CIC, multiplied by $E^{2.5}$ compared with results of other experiments; the continuous lines above and below the spectrum are the error envelopes and show combined statistical and systematic uncertainties; the energy range used for plotting starts from the maximum efficiency threshold (fig. 3).

ACKNOWLEDGMENTS

REFERENCES

1. A.M. Hillas et al., Proc.12th ICRC, Hobart 3 (1971) 1001
2. D.M. Edge et al., *J. Phys. A: Math. Nucl.* Gen.6 (1973) 1612; M. Nagano et al., *J. Phys. G:Nucl. Part. Phys.*10(1984) 1295; Y. Dai et al., *J.Phys.G: Nucl. Part. Phys*. 14(1998) 793; M. Roth et al.- Auger collaboration Proc. 28th ICRC, Tsukuba, Japan, vol. 2 (2003) 333
3. A. Haungs et al., KASCADE-Grande collaboration, Proc. 28th ICRC, Tsukuba, Japan, vol.2 (2003)985
4. H. Rebel and O. Sima et al. KASCADE-Grande collaboration, Proc. 29th ICRC, Pune, India, vol.6 (2005)297 I.M. Brancus et al. KASCADE-Grande collaboration, Proc. 29th ICRC, Pune, India, vol.6 (2005)361
5. O. Sima et al., Report FZKA 6985, Forschungszentrum Karlsruhe 2004
6. G. Toma et al., Proc. 26th ECRS 2006, Lisbon, Portugal, so-134; CERN program library, GEANT users guide, (1997)
7. J. Linsley et al., *Journ. Phys. Soc. Japan* 17 (1962) A-III